Free Carrier Generation and Recombination in PbS Quantum Dot solar cells

Jona Kurpiers[1], Daniel M. Balazs[2], Andreas Paulke[1], Steve Albrecht[1,3], Ilja Lange[1], Loredana Protesescu[4,5], Maksym V. Kovalenko[4,5], Maria Antonietta Loi[2] and Dieter Neher[1,*]

[1]*Institute of Physics and Astronomy, Soft Matter Physics, University of Potsdam, Karl-Liebknecht-Str. 24-25, 14476 Potsdam, Germany*

[2]*Photophysics and Opto Electronics - Zernike Institute for Advanced Materials, Nijenborgh 4, 9747 AG Groningen, The Netherlands*

[3]*Present address: Helmholtz-Zentrum Berlin für Materialien und Energie GmbH, Institut für Silizium-Photovoltaik, Kekuléstrasse 5, 12489 Berlin, Germany*

[4]*Department of Chemistry and Applied Biosciences, ETH Zürich, Vladimir Prelog Weg 1, Zürich, 8093, Switzerland*

[5]*Empa-Swiss Federal Laboratories for Materials Science and Technology, Überlandstrasse 129, Dübendorf, 8600, Switzerland*

Time Delayed Collection Field (TDCF) and Bias Assisted Charge Extraction (BACE) experiments are used to investigate the charge carrier dynamics in PbS colloidal quantum dot solar cells. We find that free charge carrier creation is slightly field dependent, thus providing an upper limit to the fill factor. BACE measurements reveal a rather high effective mobility of 2×10^{-3} cm²/Vs, meaning that charge extraction is efficient. On the other hand, a rather high steady state non-geminate recombination coefficient of 3×10^{-10}cm³/s is measured. We, therefore, propose rapid free charge recombination to constitute the main origin for the limited efficiency of PbS colloidal quantum dots cells.

Colloidal quantum dots (CQDs) are a promising class of materials for optoelectronic applications due to their well-tunable optical and electronic properties. In the last years improvement in the quality of the CQDs, as a consequence of better and cleaner synthetic processes, has stimulated their use in a variety of applications from light emitting diodes[1] to solar cells[2,3], field effect transistors[4-6] and photocatalytic devices[7,8]. The size-induced quantum confinement in the quantum dots can be tuned via precise tuning of the QDs dimensions. This quantum confinement can be partially maintained even in strongly coupled CQD solids[9]. Strong coupling is achieved through the ligand exchange process, by which the original, bulky organic ligands are replaced with shorter ones, enhancing the electronic coupling. Lead chalcogenide quantum dot solids exhibit a very broad absorption range, extending into the near infrared region[10]. This makes them particularly attractive for photovoltaic devices with high photocurrents[11]. From the early Schottky devices[9,11], which show limited open circuit voltage (V_{oc}) and fill factors (*FF*), great improvement in the device structure and in the choice of ligands led to a record PbS CQD solar cell with efficiencies up to 10%. That record device showed a short circuit current of up to 22 mA/cm^2, V_{oc} of 0.63 V and *FF* of 0.7 [12]. Still, the device performance seems to be limited by the V_{OC} and the *FF*, purportedly due to recombination

assisted by a large number of traps[13] or geminate recombination[14]. The nature of traps and the recombination mechanism in CQD solar cells is not yet fully understood.

To date, most works have focused on the transport in CQD solids[15-17] or the photophysics[18], and only a few have investigated the working mechanisms of CQD solar cells in detail[14,19,20]. In this letter, we use time-delayed collection field (TDCF)[21], bias-assisted charge extraction (BACE)[22] and steady state measurements to investigate free charge generation and recombination in PbS CQDs Schottky structure solar cells. We find charge generation to be slightly field-dependent, charge extraction to be reasonably efficient and free charge loss to be dominated by bimolecular recombination.

Schottky-junction solar cells based on 3.8 nm PbS CQDs were fabricated following the procedure described in the Experimental section. The *JV*-curve and parameters of the device investigated here are shown in supplemental Figure S1[23]. Bias assisted charge extraction (BACE) was utilized to measure the carrier density in the devices at V_{oc} under different illumination conditions. In BACE, the sample is illuminated with a constant light intensity for ca. 3 ms to reach steady state. Then, the illumination is switched off and a reverse bias is applied to extract all mobile carriers from the active layer. A blue 445 nm cw-laser diode was used as a light source. To avoid carrier losses due to free carrier recombination, the illumination was switched-off within 10 ns while the external bias was switched from V_{oc} to the collection bias V_{coll} simultaneously. Figure 1b) shows the resulting carrier density as a function of the steady state light intensity.

At V_{oc}, the net current in the device is zero, meaning that all photogenerated carriers must recombine. If the generation rate G is proportional to light intensity and independent of field, the extracted charge density n as function of illumination intensity at the respective V_{oc} yields the order of recombination via:

$$n = \left(\frac{G}{k_\alpha} \right)^{1/\alpha} \qquad (1).$$

The data in Figure 1b, plotted in a log-log-fashion, approximate a slope of ½ for higher illumination intensities, in accordance with a strict bimolecular recombination process (recombination order $\alpha = 2$) with a density independent free carrier recombination coefficient k_2. At lower illumination intensities, the extracted charge carrier density is expected to deviate from the true average carrier density in the active layer, due to an inhomogeneous charge distribution[24]. Therefore, results for illumination intensities below ca. 1 sun (100 mW/cm^2) have been omitted. To determine the absolute value of k_2, the generation rate was estimated from the saturated reverse photocurrent J_{sat}. With $J_{sat} = 20$ mA/cm² at an illumination intensity of at AM1.5G at 100 mW/cm^2 a reverse bias of -1.5 V and an active layer thickness d of 140 nm, $k_2 = 3 \times 10^{-10}$ cm³/s. This value is significantly larger than for most organic donor-acceptor blends, for which k_2 is typically between 10^{-12} and 10^{-11} cm^3/s[21,25-27]. As a consequence of rapid free carrier recombination, the charge density in the device extrapolated to 1 sun illumination intensity is fairly small, around $n = 5 \times 10^{15}\,\mathrm{cm}^{-3}$, while polymer-based bulk heterojunction cells typically exhibit n in excess of 10^{16} cm^{-3}, [22,28,29].

As stated, at V_{OC} all photogenerated carriers must undergo recombination. Thus, the losses in voltage from the bandgap to V_{OC} are due to recombination of some form or another. We propose that this rapid free carrier recombination and the resulting low steady state carrier density at an illumination intensity of one sun is a major reason for the low V_{OC} and underperformance of these cells.

Despite the rather high coefficient for free carrier recombination, our devices exhibit a reasonably high FF, meaning that photogenerated charges are rapidly extracted from the active layer, even at low internal fields. This is perhaps surprising as recombination and charge extraction are in competition with each other within the operating regime of a solar cell. Thus, high FFs imply efficient charge extraction in spite of strong recombination, which suggests high charge carrier mobilities. Balazs et al.[30] reported impressively high field effect transistor (FET) electron mobilities ~10^{-2} cm²/Vs in colloidal quantum dot solids, but hole mobilities

that were rather low, ~10^{-4} cm²/Vs. Mobilities for CQDs with BDT ligand, measured in field effect transistors by Bisri et al., were significantly lower[31], but these FET mobilities were shown to be strongly affected by traps at the interface between the CQD layer and the gate dielectric[31] and can be improved by 5 orders of magnitude using an ion gel gating[31]. Thus mobilities in the FET architecture are not necessarily applicable for understanding solar cell operation.

We have recently proposed an approach to determine effective charge carrier mobility $\mu_{eff} = \frac{2\mu_e\mu_h}{\mu_e + \mu_h}$ within a solar cell at working conditions, which relies on the measurement of the V_{OC} and JV characteristics at varying charge carrier densities. To be more specific, a certain carrier density n is established in two ways: either by illumination at intensity I_1 and V_{OC} conditions, where the net-current density is zero or by keeping the device at a lower bias V < V_{OC}, but at higher illumination intensity I_2, with a measurable net-current $J(V)$. With these data, the effective mobility is calculated via Eq. (2)[29]:

$$\mu_{eff}(n,V) = \frac{J(V)d}{2en(V)(V_{oc} - V)} \qquad (2)$$

Figure 1c summarizes values for the steady state carrier densities at open circuit, $n(V_{oc})$, measured with increasing illumination intensity, together with $n(V)$ for a fixed illumination intensity corresponding to a short circuit current of 24 mA/cm^2. ***$n(V_{oc})$ increases exponentially with V_{oc} at increased intensities, as expected and shown before[22,29]. In contrast, at a given intensity, n(V) varies more smoothly with bias. By definition, n(V) intersects with $n(V_{oc})$ at the particular V_{oc}, but it decreases gradually when the bias is below V_{oc} due to more rapid extraction of the carriers. In the working range of solar cells,*** $\mu_{eff,}$ as derived from these data with Eq. 2, varies between $1.5-3\times10^{-3}$ cm²/Vs, slightly depending on bias and illumination intensity. The mobility, influenced by both the holes and electrons, compares well to that of some high FF organic solar cells[22,29]. For comparison, we have estimated the mobility of the faster carrier type from the initial decay of the photocurrent transients (see Figure S2), which yielded a value of $\mu_{TDCF} = 8\times10^{-3}$ cm²/Vs. In view of the results by Bisri et al discussed above, we assign this to the motion of electrons. As μ_{eff} is markedly lower than μ_{TDCF} we conclude that the extraction of photogenerated charges out of the active layer is limited by the slow motion of holes.

In addition to issues with charge extraction, the FF can be limited by the field dependence of charge generation. To check for such dependence, TDCF experiments were conducted as a function of excitation wavelength and bias. Experiments were performed with excitation wavelengths of 410 and 532 nm, using a delay of only 4.5 ns between pulsed illumination and initiation of charge extraction with an applied V_{coll} of -1.5 V. This delay was chosen to ensure free carrier recombination had not yet commenced. For these conditions, we found the extracted charge to scale strictly linearly over a wide range of fluences (between 0.005 µJ/cm² and 0.7 µJ/cm²), ruling out any significant losses by higher order processes (Figure S3). In the following, the efficiency of generation (EGE), expressed by the total extractable charge Q_{tot} in relation to the number of incident photons, is discussed at a rather low fluence (of only 0.15 µJ/cm²), as this yielded a charge carrier density comparable to steady state conditions under one sun. Charge generation with excitation wavelength of 532 nm was found to have a slight field dependence, which becomes somewhat stronger if the sample is instead excited at 410 nm (Figure S3). An EGE of 0.5 at short circuit conditions indicates that 50% of the incident photons yield collected charges, and that at reverse bias this improves to almost 55% as the stronger electric field suppresses geminate recombination. The field dependent external generation data is overlaid on the steady state JV characteristics in Figure 1d. It becomes clear that when driving the device at reverse bias, the increasing photocurrent can be directly attributed to the improved generation efficiency at these stronger fields, and reduced free carrier recombination. However, as the device approaches V_{oc} the current becomes more strongly affected by the internal electrical field, which

cannot be ascribed entirely to generation, but rather is attributed to free carrier recombination (light area in Figure 1d).

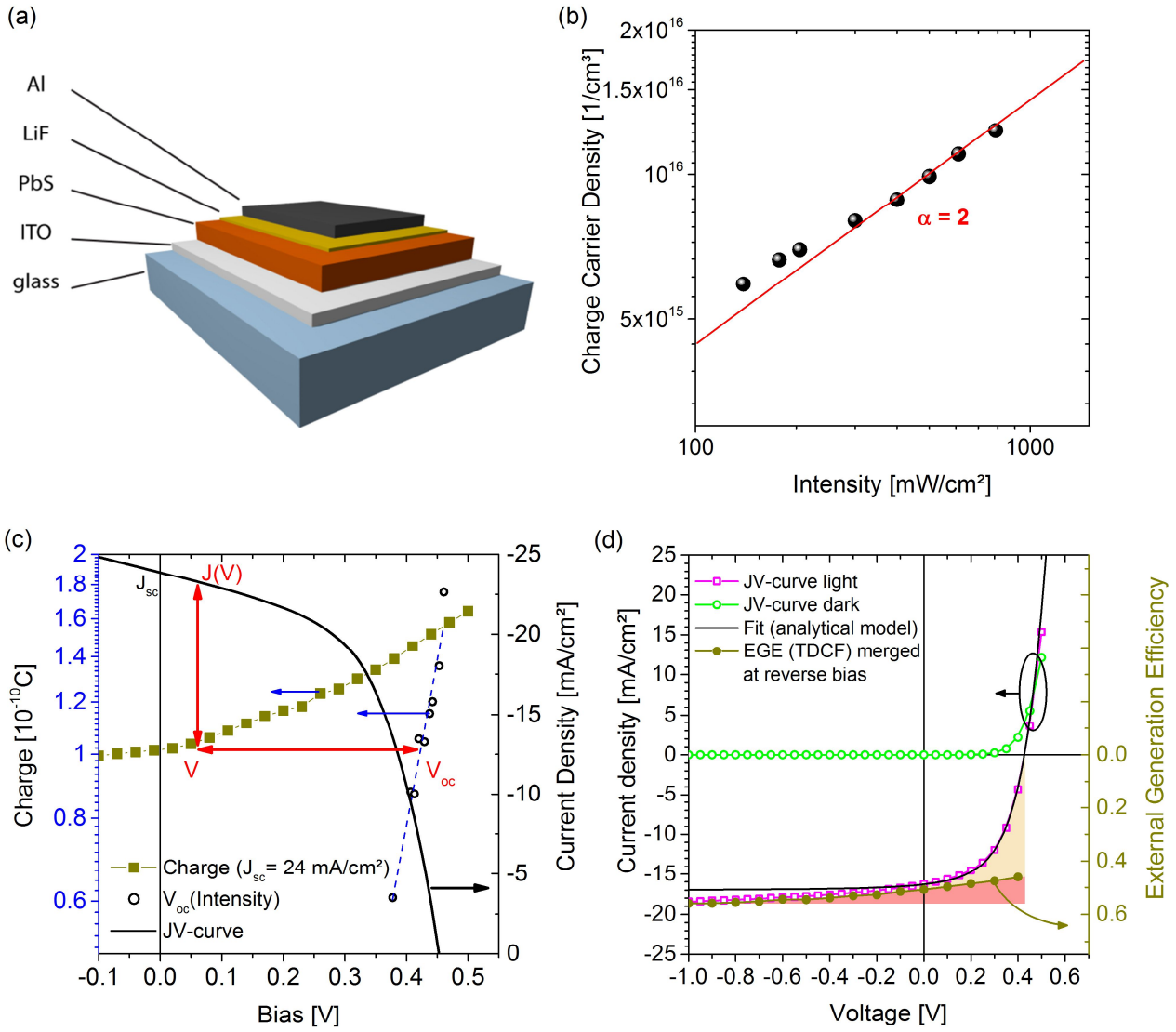

Figure 1 (a) Schematic device structure, the PbS QDs are cross-linked with BDT. (b) Charge carrier density measured with BACE at different illumination intensities at a bias which equals V_{oc} (black circles), with the red line showing the slope for strict bimolecular recombination, with a recombination coefficient $k_2 \sim 3\times10^{-10}$ cm³/s. (c) BACE measurements of the steady state carrier density at different illumination conditions in the operating voltage range. Shown are measurements with increasing intensity at V_{oc} (black circles) and at a fixed intensity (yielding a short circuit current of 24 mA/cm^2, dark yellow squares). The corresponding *JV*-curve is shown by a black solid line. *V* is the bias were the charge carrier density *n* corresponding to the current *J*(*V*) was obtained. (d) Bias dependent current in the dark (open green circles) and at AM1.5G (pink open squares), compared to the field dependence of free charge generation measured with TDCF (wavelength 532 nm, delay time 4.5 ns, dark yellow circles). The area above the measured EGE shows non-geminate and the area below geminate losses. The solid line is the prediction from an analytical model based on experimentally determined parameters.

To check for consistency between the data gained by the BACE and steady state *JV* measurements, in Figure 1d the experimental *JV*-curve is compared to an analytical model based on second order recombination, as published recently by U. Würfel and D. Neher[32]. Here, the current density J and the external bias V_{ext} are written as functions of the internal voltage V_{int}, where V_{int} is a direct measure of the quasi-Fermi level splitting in the bulk of the photoactive material:

$$J(V_{\text{int}}) = J_0\left\{\exp\left[\frac{eV_{\text{int}}}{k_B T}\right]-1\right\} - J_G \qquad (3a)$$

$$V_{ext}(V_{\text{int}}) = V_{\text{int}} + \frac{d}{2e\mu_{eff}\exp\left[\frac{eV_{\text{int}}}{2k_B T}\right]} J(V_{\text{int}}) \qquad (3b)$$

Here, J_G is the generation current, k_B Boltzmann's constant, T the temperature and $J_0 = edk_2 n_i^2$ is the saturation current density which depends on e the elementary charge, k_2 the recombination rate and n_i the intrinsic charge carrier density. To calculate $J(V)$, k_2 and μ_{eff} were taken directly from the BACE measurements, n_i was taken from extrapolating the high charge carrier density range measured with BACE to $V_{oc} = 0$ V (see Figure S4 and Table S1), and J_G was set equal to the short circuit current (values are given in Table S1). Note that this approach does not implement field dependent charge generation. Finally, Despite the simplicity of the approach, very good agreement between the measured *JV*-curve and the prediction by the analytical model is seen (solid black line in Figure 1d), using the measured parameters (see Table S1). The model works particularly well at forward bias, where the *JV*-curve is mainly governed by non-geminate recombination.

TDCF experiments with longer delays afford a detailed look at the free charge dynamics following a pulsed excitation. Figure 2a displays the three relevant quantities, the charge flowing out of the device during pre-bias, Q_{pre}, the charge collected upon application of the reverse collection voltage, Q_{coll}, and the sum, Q_{tot}, plotted as function of delay time. Data were assembled for three different fluences, and all quantities were normalized to the total collected charge at the shortest delay time. Also, before each series of measurements, the charges present in the dark at the given pre-bias, Q_{dark} were measured. A more detailed description of this technique and analysis can be found elsewhere[21]. With increasing delay time, Q_{pre} increases continuously, as more and more charge carriers leave the device before the collection bias is applied. On the other hand, Q_{coll} exhibits a continuous decrease, as the charge left in the device after t_{del} becomes diminished by both extraction and non-geminate recombination. Thus, the drop of Q_{tot} with increasing delay denotes only the loss of charges to non-geminate recombination.

We performed TDCF measurements at a forward bias where injection is reasonably small compared to the photo-generated charge (e.g. $V_{\text{pre}} = 0.3$ V). The delay was continuously increased up to 2 μs, at which Q_{coll} is no longer detectable and Q_{tot} reaches a constant value. Interestingly, the course of the normalized Q_{tot} as function of t_{del} is nearly independent of fluence, meaning that non-geminate recombination after pulsed illumination initially does not depend on charge density. This implies recombination follows a recombination order of one ($\alpha = 1$, see Figure 2b, gray lines), which denotes a monomolecular decay process. This is in clear contrast to the results from steady state BACE outlined above, which showed non-geminate recombination (NGR) to be bimolecular under steady state illumination conditions above 1 sun illumination intensity. It suggests that the initial decay of the photogenerated free carriers in TDCF may involve (initially empty) traps. Reported trap densities, N_{T}, in PbS CQD are typically quite high, ranging between 10^{16} and 10^{17} depending on the type and density of the ligand[33]. A closer look at the TDCF data, however, reveals that the decay characteristics are inconsistent with a simple first order decay process. If trapping and recombination are strictly monomolecular processes with a time-independent first order recombination coefficient k_1, then the incremental reduction of Q_{tot} with delay time would follow the equation

$$\frac{\left[Q_{coll}(t+\Delta t) - Q_{coll}(t)\right] + \left[Q_{pre}(t+\Delta t) - Q_{pre}(t)\right]}{\Delta t} = \frac{\Delta Q_{tot}}{\Delta t} = -k_1 Q_{coll} \qquad (4).$$

This is, however, not consistent with the measured decay dynamics (Figure S5, red dashed line). To further understand the recombination order and dynamics in this system, an approach was adopted to analyze the non-geminate recombination loss, following the procedure outlined in Ref[34]. In short, the incremental change of Q_{tot} over a time increment, $\Delta Q_{tot}(t)/\Delta t$, is plotted versus $Q_{coll}(t)$ in a log-log fashion. Note that $\Delta Q_{tot}(t)$ is the loss due to NGR and $Q_{coll}(t)$ is the charge remaining in the device at time t. Therefore, for any given delay time, the slope of $\log(\Delta Q_{tot}(t)/\Delta t)$ versus $\log(Q_{coll}(t))$ yields the order of NGR. In fact, at short delays, when Q_{coll} is high, the slope of the line of best fit for the three fluences indeed gives $\alpha = 1$ (Figure 2b, grey line), which indicates a first order recombination process.

However, if the system followed a simple recombination process with a time-independent recombination coefficient, meaning that the recombination rate is an exclusive function of the charge density in the device, all points in the differential decay plot would fall on a single curve, which is clearly not the case (Figure 2b). At short delays, all three fluences deviate significantly from the single common curve traced out at longer delays.

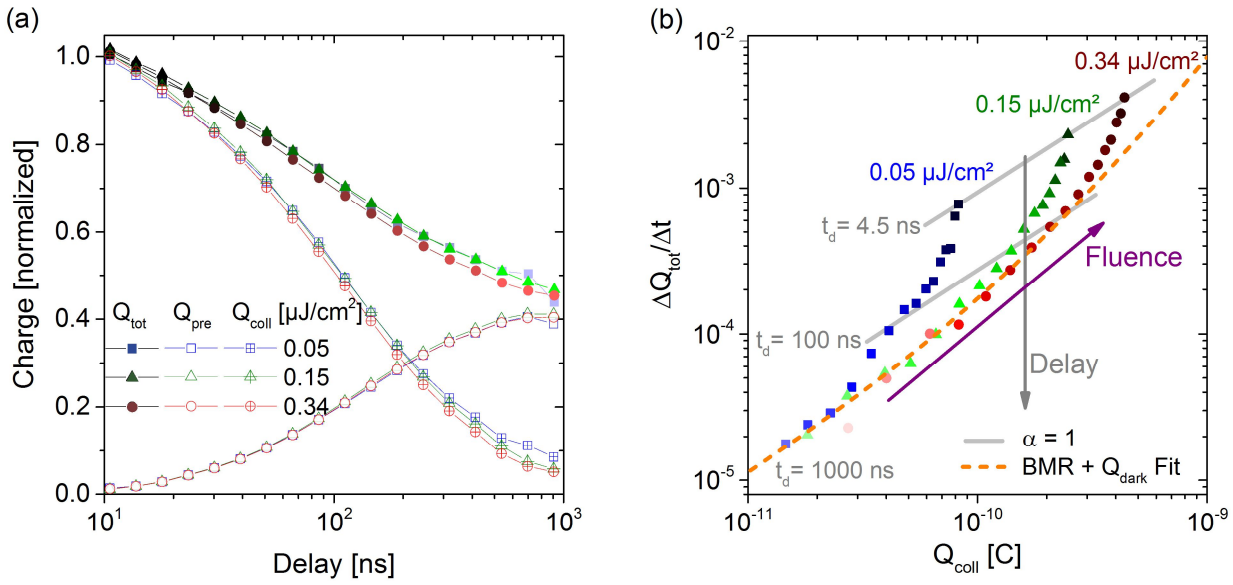

Figure 2 (a) TDCF experiments with increasing delay measured for three different fluencies; 0.05 (green), 0.15 (dark yellow), 0.34 (blue) µJ/cm² at V_{pre}=0.3 V (b) a direct plot of the recombination order, which is two for longer delays and one (gray line) for all others. The fit (dashed orange line, equation (5) is done with k_2 = 1.5x10^{-10} m³/s and Q_{dark} = 8x10^{-11} C.

A consistent explanation of both facts is that the NGR dynamics up to 100 ns is governed by a first-order process, which gradually slows down with time. Although we cannot be sure about the physical processes governing this phenomenon, we propose that the initial rapid decay may be due to trapping of the faster carrier while trapping and free carrier recombination of the slower carrier dominates the dynamics at longer times. For even longer delays, all $\Delta Q_{tot}(t)/\Delta t$ versus $Q_{coll}(t)$ data finally approach one common curve, which now follows strict bimolecular recombination in presence of dark charge, according to Eq. (4)

$$\frac{\Delta Q_{tot}}{\Delta t} = \frac{1}{eAd} k_2 (Q_{coll}^2 + 2 Q_{coll} Q_{dark}) \qquad (5).$$

Here, 8×10^{-11} C is the dark charge as determined by BACE experiments on the same device in the dark. The value for $k_2 = 1.5 \times 10^{-10}$ cm³/s from TDCF is slightly smaller than when determined by BACE.

However, this is quite understandable considering the much lower carrier densities present in the device at long delays.

The data presented above reveal rather complex charge carrier dynamics in our PbS QD dot solar cells. While the properties under steady state illumination at and above one sun (carrier density as a function of the illumination intensity, *JV*-characteristics) are consistent with strict bimolecular recombination, transient photocurrent data indicates the involvement of traps. A simple way to independently determine the order of recombination is to measure V_{oc} at different steady state intensities I, with the result shown in Figure S6. In this semilogarithmic presentation, the slope of the V_{oc} - $\ln(I/I_0)$ plot is $2k_BT/\alpha q$, where α is the order of the recombination process and k_BT/q is the thermal voltage. In case of pure bimolecular recombination, $\alpha = 2$, while $\alpha = 1$ for trap-assisted recombination. Consistent with results on other CQD solar cells[35,36], our measurements reveal two distinct ranges. While at low intensities the role of the traps is dominant, α approaches a value of 2 above one sun illumination intensity. This indicates direct free carrier recombination dominates at solar illumination conditions, in full agreement with the BACE results outlined above.

Our studies reveal a conclusive picture of the processes determining the steady state *JV*-curves of PbS based CQD solar cells. Specifically, time-delayed collection field experiments reveal a weak yet distinct field-dependence of generation, setting an upper limit to the achievable fill factor. Transient and low intensity steady state measurements highlight the role of traps, but non-geminate recombination is found to be strictly bimolecular at application relevant steady state conditions, with a high bimolecular recombination coefficient of 3×10^{-10} cm³/s. As a consequence of the fast non-geminate recombination loss, carrier densities at open circuit condition are fairly low, going along with a large V_{oc} loss of ca. 0.75 V (with respect to a bandgap of 1.18 eV). On the other hand, the rather high effective mobility of ca. 2×10^{-3} cm²/Vs, measured under steady state illumination, allows for fast extraction and ensures a reasonably high fill factor, despite fast non-geminate recombination.

J.K. wants to thank John Love for kindly revising the manuscript. This work was funded by the Deutsche Forschungsgesellschaft (DFG) Projekt Nr. NE 410/13-1, NE410/15-1 and INST 336/94-1 FUGG. D.M.B, L.P, M.V.K and M.A.L are grateful for the financial support of the European Research Council (ERC Starting Grant "HySPoD" No. 306983 in Groningen and "NANOSOLID" No. 306733 in Zurich).

J.K., M.A.L and D.N. wrote the main manuscript text, L.P, synthesized the quantum dots, D.M.B. prepared the devices, J.K., S.A. and I.L. performed the experiments and prepared the figures. All authors reviewed the manuscript.

1 Y. Shirasaki, G. J. Supran, M. G. Bawendi, and V. Bulovic, Nat Photonics **7** (1), 13 (2013).

2 C. H. M. Chuang, P. R. Brown, V. Bulovic, and M. G. Bawendi, Nat Mater **13** (8), 796 (2014).

3 Z. J. Ning, O. Voznyy, J. Pan, S. Hoogland, V. Adinolfi, J. X. Xu, M. Li, A. R. Kirmani, J. P. Sun, J. Minor, K. W. Kemp, H. P. Dong, L. Rollny, A. Labelle, G. Carey, B. Sutherland, I. G. Hill, A. Amassian, H. Liu, J. Tang, O. M. Bakr, and E. H. Sargent, Nat Mater **13** (8), 822 (2014).

4 F. Hetsch, N. Zhao, S. V. Kershaw, and A. L. Rogach, Mater Today **16** (9), 312 (2013).

5 D. K. Kim, Y. M. Lai, B. T. Diroll, C. B. Murray, and C. R. Kagan, Nature communications **3** (2012).

6 M. I. Nugraha, R. Hausermann, S. Z. Bisri, H. Matsui, M. Sytnyk, W. Heiss, J. Takeya, and M. A. Loi, Adv Mater **27** (12), 2107 (2015).

7 L. H. Lai, W. Gomulya, M. Berghuis, L. Protesescu, R. J. Detz, J. N. H. Reek, M. V. Kovalenko, and M. A. Loi, Acs Appl Mater Inter **7** (34), 19083 (2015).

8 L. H. Lai, W. Gomulya, L. Protesescu, M. V. Kovalenko, and M. A. Loi, Phys Chem Chem Phys **16** (16), 7531 (2014).

9 G. I. Koleilat, L. Levina, H. Shukla, S. H. Myrskog, S. Hinds, A. G. Pattantyus-Abraham, and E. H. Sargent, Acs Nano **2** (5), 833 (2008).

10 C. Piliego, L. Protesescu, S. Z. Bisri, M. V. Kovalenko, and M. A. Loi, Energ Environ Sci **6** (10), 3054 (2013).

[11] K. Szendrei, W. Gomulya, M. Yarema, W. Heiss, and M. A. Loi, Appl Phys Lett **97** (20) (2010).

[12] X. Lan, O. Voznyy, A. Kiani, G. d. A. F. Pelayo, A. S. Abbas, G. Kim, M. Liu, Z. Yang, G. Walters, J. Xu, M. Yuan, Z. Ning, F. Fan, P. Kanjanaboos, I. Kramer, D. Zhitomirsky, P. Lee, A. Perelgut, S. Hoogland, and E. H. Sargent, Adv Mater, n/a (2015).

[13] M. J. Speirs, D. M. Balazs, H. H. Fang, L. H. Lai, L. Protesescu, M. V. Kovalenko, and M. A. Loi, J Mater Chem A **3** (4), 1450 (2015).

[14] A. A. Bakulin, S. Neutzner, H. J. Bakker, L. Ottaviani, D. Barakel, and Z. Y. Chen, Acs Nano **7** (10), 8771 (2013).

[15] Y. Liu, M. Gibbs, J. Puthussery, S. Gaik, R. Ihly, H. W. Hillhouse, and M. Law, Nano Lett **10** (5), 1960 (2010).

[16] P. T. Erslev, H. Y. Chen, J. B. Gao, M. C. Beard, A. J. Frank, J. van de Lagemaat, J. C. Johnson, and J. M. Luther, Phys Rev B **86** (15) (2012).

[17] J. M. Luther, M. Law, Q. Song, C. L. Perkins, M. C. Beard, and A. J. Nozik, Acs Nano **2** (2), 271 (2008).

[18] J. B. Gao and J. C. Johnson, Acs Nano **6** (4), 3292 (2012).

[19] K. Szendrei, M. Speirs, W. Gomulya, D. Jarzab, M. Manca, O. V. Mikhnenko, M. Yarema, B. J. Kooi, W. Heiss, and M. A. Loi, Adv Funct Mater **22** (8), 1598 (2012).

[20] C. H. M. Chuang, A. Maurano, R. E. Brandt, G. W. Hwang, J. Jean, T. Buonassisi, V. Bulovic, and M. G. Bawendi, Nano Lett **15** (5), 3286 (2015).

[21] S. Albrecht, W. Schindler, J. Kurpiers, J. Kniepert, J. C. Blakesley, I. Dumsch, S. Allard, K. Fostiropoulos, U. Scherf, and D. Neher, J Phys Chem Lett **3** (5), 640 (2012).

[22] J. Kniepert, I. Lange, J. Heidbrink, J. Kurpiers, T. J. K. Brenner, L. J. A. Koster, and D. Neher, Journal of Physical Chemistry C **119** (15), 8310 (2015).

[23] See supplemental material at [URL will be inserted by AIP] for JV-curves, mobility data, field dependence of charge generation measurements, charge carrier dynamics and steady state recombination.

[24] F. Deledalle, P. S. Tuladhar, J. Nelson, J. R. Durrant, and T. Kirchartz, Journal of Physical Chemistry C **118** (17), 8837 (2014).

[25] J. Kniepert, M. Schubert, J. C. Blakesley, and D. Neher, J Phys Chem Lett **2** (7), 700 (2011).

[26] Alexander Foertig, Juliane Kniepert, Markus Gluecker, Thomas Brenner, Vladimir Dyakonov, Dieter Neher, and Carsten Deibel, Adv Funct Mater **24** (9), 1306 (2014).

[27] D. Rauh, C. Deibel, and V. Dyakonov, Adv Funct Mater **22** (16), 3371 (2012).

[28] I. Lange, J. Kniepert, P. Pingel, I. Dumsch, S. Allard, S. Janietz, U. Scherf, and D. Neher, J Phys Chem Lett **4** (22), 3865 (2013).

[29] S. Albrecht, J. R. Tumbleston, S. Janietz, I. Dumsch, S. Allard, U. Scherf, H. Ade, and D. Neher, J Phys Chem Lett **5** (7), 1131 (2014).

[30] D. M. Balazs, M. I. Nugraha, S. Z. Bisri, M. Sytnyk, W. Heiss, and M. A. Loi, Appl Phys Lett **104** (11) (2014).

[31] S. Z. Bisri, C. Piliego, M. Yarema, W. G. Heiss, and M. A. Loi, Adv Mater **25** (31), 4309 (2013).

[32] U. Würfel, D. Neher, A. Spies, and S. Albrecht, Nature communications **6**, 6951 (2015).

[33] A. H. Ip, S. M. Thon, S. Hoogland, O. Voznyy, D. Zhitomirsky, R. Debnath, L. Levina, L. R. Rollny, G. H. Carey, A. Fischer, K. W. Kemp, I. J. Kramer, Z. J. Ning, A. J. Labelle, K. W. Chou, A. Amassian, and E. H. Sargent, Nat Nanotechnol **7** (9), 577 (2012).

[34] A. Paulke, S. Stranks, J. Kniepert, J. Kurpiers, C. Wolff, N. Schön, H. Snaith, T. J. K. Brenner, and D. Neher, Appl Phys Lett **submitted** (2016).

[35] W. L. Leong, S. R. Cowan, and A. J. Heeger, Adv Energy Mater **1** (4), 517 (2011).

[36] T. M. Clarke, C. Lungenschmied, J. Peet, N. Drolet, and A. J. Mozer, Adv Energy Mater **5** (4) (2015).